Investigation of the mechanism of emergence of autowave structures at the reaction front

Eduard O. Yakupov,[1,*] Andrey A. Polezhaev,[1,2,†] Vladimir V. Gubernov,[1,‡] and Taisia P. Miroshnichenko[1,§]
[1]*P. N. Lebedev Physical Institute of the Russian Academy of Sciences, 53 Leninskiy Prospekt, Moscow, Russia*
[2]*Peoples Friendship University of Russia (RUDN University), Moscow, Russia*

(Received 7 February 2019; revised manuscript received 1 April 2019; published 25 April 2019)

A qualitative mechanism for autowave pattern formation at the reaction front, observed in certain chemical systems including combustion, is suggested. It is assumed that patterns are formed as a result of interaction of two subsystems, one of which is responsible for the reaction front propagation while the other determines the formation of waves at the front. A corresponding phenomenological model is constructed in which reaction front propagation is described by a submodel of the Fisher-Kolmogorov-Petrovskii-Piskunov type and waves on the front are described by a submodel of the FitzHugh-Nagumo type. In the three-dimensional numerical analysis, it is demonstrated that the model is able to qualitatively explain the emergence of wave patterns of both spiral and target types, which are experimentally observed at the reaction front. The dependence of these patterns on the velocity and thickness of the front is examined.

DOI: 10.1103/PhysRevE.99.042215

I. INTRODUCTION

There are numerous examples of nonlinear reaction-diffusion systems, which support the formation of complex spatiotemporal structures in systems of different nature [1–11]. These include traveling, pulsating, chaotic, quasiperiodic, target, spiral, cellular waves, oscillons, soliton-like waves, etc., which may also exhibit diverse dynamical behavior. All these regimes are observed in chemical systems, which provide a convenient tool for both experimental and theoretical study.

In some cases, chemical reactions proceed not uniformly in space but in the form of a propagating front. Among them are the reaction between the initially spatially separated reagents forming as the result insoluble precipitating matter, usually nonuniformly distributed (the so-called Liesegang structures) [12], and self-propagating high-temperature synthesis (SHS) [13]. Another vivid example is propagation of a combustion front. In combustion systems, the emergence of nonlinear wave patterns may be due to diffusion-thermal instabilities [14–16] or hydrodynamic instabilities [9,17]. The onset of instabilities may also be enhanced due to the flame-wall or burner [18,19] or flame-flow interaction [11,20].

In this work, we mainly focus on the case of the diffusion-thermal instabilities as the source of the nonlinear waves. The onset of the diffusive-thermal instabilities is known to be due to imbalance of diffusive fluxes of heat and reactants, which is quantified by the Lewis number [21]. In the case when the Lewis number is less than one, the cellular or more common term for nonlinear dynamics, the Turing type, of instabilities occurs, leading to the formation of flame corrugation or cells in the direction transverse to the direction of flame propagation. For Lewis numbers greater than one, the flame front exhibits the emergence of the traveling or pulsating instabilities, which result in the formation of different unsteady regimes of combustion.

In Refs. [18,19,22–27], the premixed hydrocarbon flames stabilized on the porous plug burner were studied experimentally, numerically, and analytically. It was found that under certain conditions the pulsating, target, spiral, and cellular waves can occur. The dynamics of these nonlinear structures can also become complex and may lead to the formation of quasiperiodic and chaotic regimes of combustion. Quantitatively and qualitatively it was demonstrated by means of asymptotic [18,26] and numerical analysis [19,27], respectively, that the emergence of traveling and cellular diffusive-thermal instabilities are responsible for the formation of such regimes.

In several studies [25,28–31], the occurrence of the pulsating, spiral, and target waves were investigated experimentally for the case of the premixed flames propagating downward in tubes of different diameters. The results were also repeated under microgravity conditions to exclude the effects of buoyancy, while leaving only the diffusive-thermal mechanism for loss of stability. In a series of experiments with the spherically expanding flames [32–34], it was demonstrated that there may appear spiral and target patterns at the surface of the symmetric radially expanding combustion wave. In these examples, there are two types of nonlinear waves, which coexist: the basic automodel traveling or expanding solution and the nonlinear structure (spiral or target waves) which appears on top of the automodel solution and propagates with it.

As for now, there are no models which can demonstrate and describe such dynamical behavior. We can mention here that in chemically reacting systems there are also cases of the structures where one type of nonlinear pattern is hosted by the other type of the nonlinear pattern. An example is the segmented waves observed in the Belousov-Zhabotinskiy

*edward.thrst@gmail.com
†apol@lpi.ru
‡v.v.gubernov@gmail.com
§taisia.miroshnichenko@gmail.com

reaction [35]. In our study, we propose a theoretical model for such phenomena of general nature, which includes two submodels. One of them describes the propagation of a traveling wave, while the other is responsible for generation of nonlinear patterns at the traveling front. This approach has already been successfully applied by us to two phenomena: models for the mechanism of segmented waves formation [36] and of oscillon (localized oscillating pattern) [37].

In the present paper, we first formulate a simple model to explain formation of wave patterns at the combustion or, more generally, at the reaction front and then demonstrate in numerical experiments that it is able to describe the formation of both target patterns and spirals. We also present the results of systematic study of the dependence of these patterns on the velocity and thickness of the reaction front.

II. MODEL

As is stated above, autowave structures at the reaction front may be viewed as a superposition of two processes: propagation of the front and the development of wave patterns at the latter. Thus, the model corresponding to this scenario should consist of two submodels describing each of these processes. We verify this hypothesis on a rather simple model in which the block responsible for appearance and movement of the reaction front is the Fisher-Kolmogorov-Petrovskii-Piskunov (F-KPP) [38,39] equation:

$$\frac{\partial g}{\partial t} = kg(1-g) + D_g \Delta g, \tag{1}$$

while patterns formed on this front are due to the model of the Fitzhugh-Nagumo (FHN) [40] type:

$$\begin{aligned} \frac{\partial u}{\partial t} &= \frac{1}{\varepsilon}[u(u-\alpha)(1-u) - v] + D_u \Delta u, \\ \frac{\partial v}{\partial t} &= u - v + D_v \Delta v. \end{aligned} \tag{2}$$

We assume that the first submodel, Eq. (1), affects parametrically the second one, Eq. (2), so that the state of the latter changes at the front from quiescent to either excitable or oscillatory. The parameter responsible for this transition is α, and we assume the following coupling equation between this parameter and the variable g:

$$\alpha = a - b(1-g)g. \tag{3}$$

The reason for choosing the F-KPP Eq. (1) for the propagating reaction front is that it is perhaps the simplest model describing a traveling wave. At the front, the corresponding variable monotonically switches from the initial to the final states. We may speculate that, on the one hand, in a real chemical system the irreversible consumption of the source substance will result in formation of such reaction front or, on the other hand, we observe similar shape of temperature profile on the front of the combustion wave. The nonlinear form of the coupling Eq. (3) reflects the idea that the first submodel [Eq. (1)] should influence the second one [Eq. (2)] only in the region where reaction takes place in Eq. (1); i.e., the source term in Eq. (1) is significantly nonzero. This approach to some extent is similar to the work [41] in a sense that the submodel (1) provides spatial modulation of the properties of the system for the submodel (2).

In Eq. (1), there are two parameters: k, D_g. The first one corresponds to the reaction rate while the second one is the diffusion coefficient. Their combinations $\sqrt{kD_g}$ and $\sqrt{D_g/k}$ (up to a factor of the order of unity) correspond to the values which have clear physical meaning—the speed of the front and its thickness respectively. Thus, further results of our numerical simulations are presented related to these very combinations.

As to the parameters of the second block, Eq. (2), they are chosen in such a way that away from the front the system is unexcitable while on the front due to the coupling, Eq. (3), spiral or circular waves can be formed. It is important for the wave formation that the diffusion coefficient of the first variable u, activator, should be significantly larger than the diffusion coefficient of the second variable v, inhibitor: $D_u \gg D_v$. In all the numerical simulations presented below, we took $D_v = 0$ and $D_u = 0.1$, the latter being close to the range of the varied diffusion coefficient D_g. Also, the characteristic time of the first equation should be much smaller than that of the second one, and thus in simulations we used $\varepsilon = 1/200$.

Though in real experiments autowave patterns are observed at an expanding spherical front [32,33], in our simulations we ignore curvature of the front, as we believe that it is not of such importance, and consider the case of a flat propagating reaction front.

We performed numerical simulations in a cubic domain with the side length $L = 10$, setting no-flux boundary conditions using the implemented code. Splitting with respect to physical processes was used. Kinetic equations were solved by the Runge-Kutta fourth-order method. Diffusion equations were solved by alternating direction implicit method. Details of the numerical scheme used are described in Appendix A.

All simulations were performed with the fixed spatial and time steps: $\Delta x = 0.1$, $\Delta t = 0.005$. The convergence of the algorithm was verified by reducing of both time and spatial steps, which resulted in essentially the same spatiotemporal behavior of solution. We verified in simulations that solutions are stable against perturbations of regular nature and with respect to the numerical noise added to the computation process.

III. RESULTS

In this section, we present the results of numerical simulations of the above-formulated model. First, we demonstrate how it is able to reproduce target patterns at the reaction front.

Front propagation is described by Eq. (1), while at the front the variable g changes from zero to unity. In this region, due to the coupling Eq. (3) the submodel Eq. (2), which is originally unexcitable, becomes excitable everywhere but in a small central region of the front, which becomes oscillatory and serves as a wave source or pacemaker. The emergence of this pacemaker may be due to possible heterogeneity or impurity at the front in real chemical system such as, for example, dust particles or the emergence of other types of instabilities (hydrodynamic instabilities) superimposed over the diffusive-thermal instabilities. Thus, in the coupling equation (3) $a = 0.6$

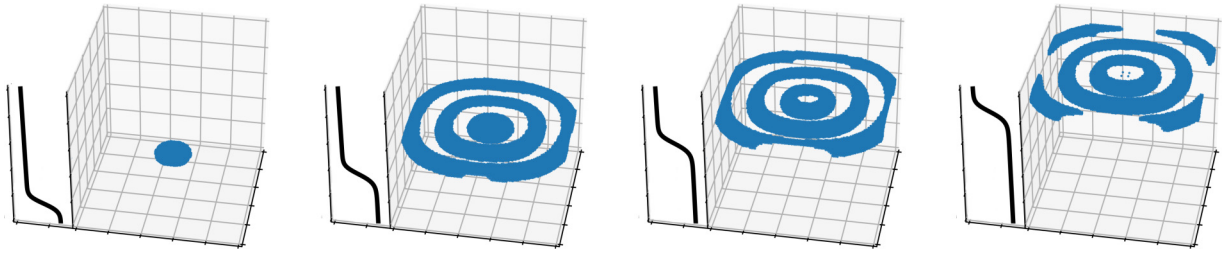

FIG. 1. Typical evolution of a target pattern at the reaction front. Parameters of Eqs. (1) and (2): $\sqrt{D_g/k} = 0.1$, $\sqrt{kD_g} = 0.350$ ($k = 3.5$, $D_g = 0.035$), $\varepsilon = 1/200$, $D_u = 0.1$, $D_v = 0.0$. The variable u is shown; color corresponds to the regions where its value is greater than 0.1. (In the rest of the space, this variable is slightly different from zero.) From the center of the reaction front, where the source of oscillations is located, circle patterns begin to form and move along with the front. The solid line on the left side of each figure corresponds to the variable g and allows us to determine the position of the reaction front.

and $b = 3$ for a wave source and $a = 0.6$ and $b = 2.2$ in the remaining region.

Typical result of numerical simulation of Eqs. (1) and (2) with such coupling is shown in Fig. 1, where the front, at which target pattern is formed (variable u), moves along vertical axis. In this and other figures, color denotes the regions where u exceeds the value 0.1.

We have performed systematic numerical investigation of the conditions for the emergence of target patterns and their shapes, depending on the reaction front parameters k and D_g, or rather, on their combinations $\sqrt{kD_g}$, which are proportional to the front velocity, and $\sqrt{D_g/k}$, which characterizes the front thickness. Results of simulations are presented in Fig. 2. In this diagram, a "plus" sign corresponds to the parameters for which target patterns are formed at the front while the "minus" sign is for the parameters for which patterns do not arise. In fact, we tried to trace the boundary between the parametric regions for which target patterns take place or not. Above

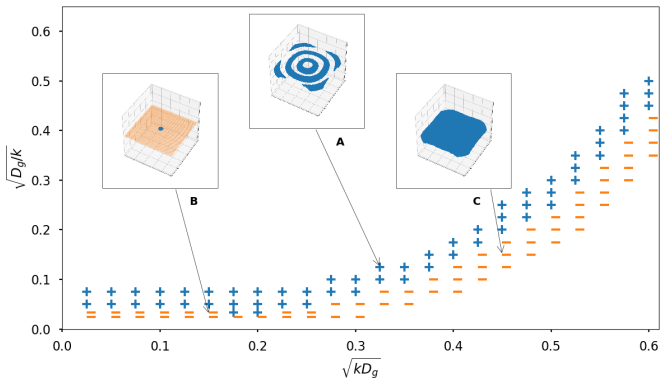

FIG. 2. The diagram showing the boundary between the region of parameters where target patterns are formed (+) and where they do not exist (−) related to the combinations $\sqrt{kD_g}$ and $\sqrt{D_g/k}$ corresponding to the speed of the front and its thickness respectively. Fixed parameters of Eqs. (1) and (2) are $\varepsilon = 1/200$, $D_u = 0.1$, $D_v = 0.0$. Characteristic types of target patterns at the reaction front: (a) normal structures, regularly releasing from the source and moving with the reaction front; (b) the case when structures are not formed, only a localized spot (associated with the source) moves with the reaction front (indicated by a different color); (c) pattern collapses and the front becomes completely excited and keeps moving as a whole.

this boundary, in Fig. 2 wave patterns are formed. However, it should be stressed that the pattern within a layer in three-dimensional (3-D) space may be treated as two dimensional (spiral or target pattern) only if the layer is thin compared to the pattern scale (pitch of the spiral or distance between rings), and as we move upwards, the front thickness increases and the pattern becomes in fact three dimensional. Below the boundary, there are no patterns.

In the left half of the plot, in the region $\sqrt{kD_g} < 0.25$, where the front speed is small, the boundary is horizontal. It means that for such velocities, the condition for target pattern formation does not depend on the speed but only on the thickness of the front. Qualitatively it can be explained in the following way. Conditions for pattern formation at the traveling wave front crucially depend on its thickness because of the reactant loss into the outer space. This loss is caused by two factors: diffusion of substances across the front and their flow (convection) through the front due to its motion. For small front velocities, the first factor dominates and thus it results in the horizontal piece of the boundary. As the front speed grows, the second factor becomes essential at $\sqrt{kD_g} \approx 0.3$ and thus the boundary tends upward, and as for pattern formation on the front its thickness should be larger for higher velocity. These qualitative considerations are supported by analysis, presented in Appendix B, of a piecewise-linear equation revealing influence of thickness of the front and its velocity on the reaction taking place in it.

From numerical simulations, we can estimate both the speed of the front and the speed of the wave at the front. When the front speed grows further and becomes approximately equal to the speed of the waves at the front, it results in total deformation of the waves which transform into a homogeneous layer, occupying the whole front. For larger front speeds, wave patterns are not formed for any front thickness.

Figures 2(a), 2(b), and 2(c) give examples of patterns for three combinations of the front parameters, indicated by arrows. Figure 2(a) illustrates normal target patterns which arise for relatively small front velocities and for sufficiently large front thickness. When the front thickness decreases to a certain value, target patterns cease to form [Fig. 2(b)]. Figure 2(c) illustrates the case of approximately equal front and wave velocities.

The model in Eqs. (1) and (2) is also able to reproduce spiral waves at the traveling front. As in the previous case, front propagation is described by Eq. (1), and patterns formed

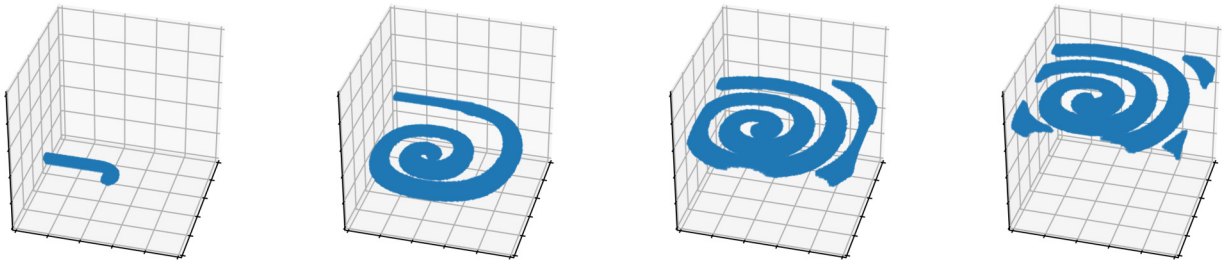

FIG. 3. Evolution of the spiral at the reaction front. The parameters used in simulations: $\sqrt{D_g/k} = 0.1$, $\sqrt{kD_g} = 0.350$ ($k = 3.5$, $D_g = 0.035$), $\varepsilon = 1/200$, $D_u = 0.1$, $D_v = 0.0$. The variable u is shown; color corresponds to the regions where its value is greater than 0.1.

on this front are due to the submodel, Eq. (2). However, now the front is uniformly excitable (there is no pacemaker, which is necessary for target patterns) and thus we take the same parameters in the coupling Eq. (3) as in the first case, $a = 0.6$ and $b = 2.2$, but now in the whole domain. Spirals emerge at the front due to appropriate initial conditions. For initial conditions in Eq. (2), we take a segment of a plane wave with a free end, which is a one-dimensional traveling-wave solution of this model with the parameter α corresponding to the excitable state. In the time course, this initial plane wave bends to form a spiral, which moves along with the front. In Fig. 3, results of numerical simulation are presented which demonstrate evolution of the initial seed wave resulting in the formation of the spiral at the traveling front.

Analysis of spiral wave formation dependent on the factor of the front thickness $\sqrt{D_g/k}$ and the factor of the front speed $\sqrt{kD_g}$ shows that the system behaves in a way similar to the previous case with target patterns. In numerical simulations, we obtain either normal spirals, rotating around the core and moving with reaction front, or the initial seed spiral extincts, or the front becomes completely excited and keeps moving as a whole.

Results of simulations are presented in Fig. 4. In this diagram, a "plus" sign corresponds to the parameters for

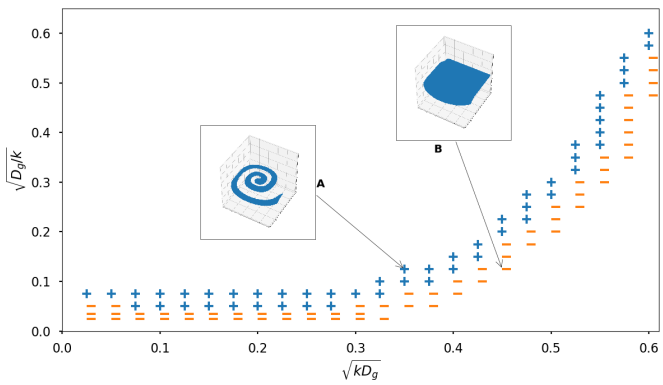

FIG. 4. The diagram showing the boundary between the region of parameters where spiral patterns are formed (+) and where they do not exist (−) related to the combinations $\sqrt{kD_g}$ and $\sqrt{D_g/k}$ corresponding to the speed of the front and its thickness respectively. Fixed parameters of Eqs. (1) and (2): $\varepsilon = 1/200$, $D_u = 0.1$, $D_v = 0.0$. Observed types of patterns at the reaction front: (a) regular rotating spirals and (b) pattern collapses and the front becomes completely excited and keeps moving as a whole.

which spiral patterns are formed at the front and a "minus" sign is for the parameters for which patterns do not arise. For relatively small values of the front velocity ($\sqrt{kD_g} < 0.3$), as we approach the boundary between "pluses" and "minuses" from above, the radius of the spiral core starts to increase and at the boundary it becomes infinite (or at least larger than the size of the domain) and the spiral vanishes. For larger values of the front speed, we observe a completely different behavior of the spiral as we approach the boundary. In this case, the velocities of the reaction front and of the spiral at this front are approximately equal, and thus as we approach the boundary the spiral is blurring and finally uniformly occupies the whole front. When we change the parameters further, we again have the case of spiral extinction.

Figures 4(a) and 4(b) illustrate typical results of evolution of the seed spiral qualitatively described above. (We do not present the case of spiral extinction, as finally there is no pattern at all.) Figure 4(a) shows normal spirals, which arise for relatively small front velocities and for sufficiently large front thicknesses. Fiugre 4(b) illustrates the case of approximately equal front and wave velocities. The arrows point out the combinations of the front parameters used in the corresponding simulations.

IV. CONCLUSION

The aim of the present study was to suggest a mechanism for formation of autowave structures at the traveling reaction front. Such patterns are observed in different chemical systems, which proceed sequentially in space, the most striking of which are combustion waves. We suppose that these patterns are formed as a result of interaction of two subsystems, one of which is responsible for the reaction front propagation while the other determines the formation of waves at the latter. Such suggestion is quite natural, as any reaction which demonstrates this phenomenon is rather complex and includes many elementary reactions and intermediate substances. Even the simplest case—combustion of oxygen—includes tens of reactions.

The suggested mechanism is verified on the example of a simple phenomenological block model in which reaction front propagation is described by a submodel of the Fisher-KPP type and waves at the front are described by a submodel of the FitzHugh-Nagumo type. Earlier, we have demonstrated [42] that this model is able to describe wave patterns at the reaction front in the two-dimensional (2-D) spatial case. In the present paper, we present results of our systematic study of this model

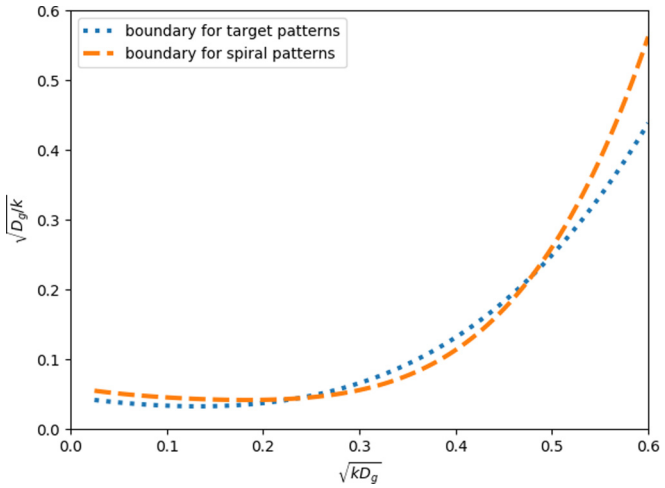

FIG. 5. Boundaries between regions in the parameter space corresponding to existence and absence of spiral (dashed line) and target (dotted line) patterns at the front.

for the three-dimensional (3-D) case. It is demonstrated that it is able to explain the experimentally observed wave patterns of both spiral and target types at the reaction front.

In addition, it is shown that the emergence of the waves at the reaction front and their shape crucially depend on the velocity and thickness of the latter. It is shown that for both spiral and target patterns to emerge at the reaction front it is necessary that the front is sufficiently thick. In both cases, the boundary between regions in the parameter space corresponding to existence and absence of wave patterns on the front in Figs. 2 and 4 is horizontal for small values of its velocity and tends upward for higher velocities, which means that the front becomes thicker, and in fact the pattern becomes three dimensional. Thus, for both cases this boundary behaves qualitatively quite similarly. To see a quantitative difference between them, we have drawn both boundaries in one plot in Fig. 5. A certain difference is observed only in the right-hand side of the plot: The boundary for target patterns goes lower than for spirals, which means that target patterns can arise in a thinner reaction front than spirals. The possible reason is the existence of a local pacemaker, which makes the conditions for pattern formation more advantageous for target patterns, at least for higher front speed.

In the current formulation, we do not expect that the results will change if we replace the leading subsystem which defines the traveling wave solution with a model of a different type. The role of this subsystem is to create certain distribution of the variable g that moves with a constant velocity along the z axis. The choice of the model would be important if we consider a feedback mechanism from the second subsystem in Eq. (2) to the first subsystem in Eq. (1). We would certainly like to undertake such analysis in future work.

In the present study, the plausibility of the proposed mechanism is verified numerically by the example of a simple phenomenological model. In the future, we plan to apply this approach to real chemical systems, demonstrating such types of patterns, especially to combustion waves.

ACKNOWLEDGMENTS

The work was supported by RFBR Grants No. 17-01-00070, No. 18-31-00411, and No. 17-53-12018. Analytical estimates and development of the numeric scheme presented in the appendix were funded by the RUDN University Program 5-100.

APPENDIX A

For solving three-dimensional unsteady reaction-diffusion equations, we use the following scheme. Equations (2) are rewritten in the form

$$\frac{\partial}{\partial t}\begin{pmatrix}u\\v\end{pmatrix} = \begin{pmatrix}\frac{1}{\varepsilon}[u(u-\alpha)(1-u)-v]\\ u-v\end{pmatrix} + \begin{pmatrix}D_u\\D_v\end{pmatrix}\Delta\begin{pmatrix}u\\v\end{pmatrix},$$

or equivalently

$$\frac{\partial \mathbf{f}}{\partial t} = \mathbf{S}(\mathbf{f},t) + \mathbf{D}\left(\frac{\partial^2 \mathbf{f}}{\partial x^2} + \frac{\partial^2 \mathbf{f}}{\partial y^2} + \frac{\partial^2 \mathbf{f}}{\partial z^2}\right), \tag{A1}$$

where $\mathbf{f}(x,y,z,t)$ is the unknown vector with the initial condition

$$\mathbf{f}(x,y,z,0) = \mathbf{f}_0(x,y,z)$$

and Neumann boundary condition

$$\frac{\partial \mathbf{f}}{\partial \mathbf{n}} = 0.$$

Then, $\mathbf{S}(\mathbf{f},t)$ is the reaction vector function and $\mathbf{D}$ is the nonnegative diagonal diffusion matrix.

First, we build the rational high-order compact alternating-direction-implicit (RHOC ADI) [43] scheme for homogeneous differential equation

$$\frac{\partial \mathbf{f}}{\partial t} = \mathbf{D}\frac{\partial^2 \mathbf{f}}{\partial x^2} + \mathbf{D}\frac{\partial^2 \mathbf{f}}{\partial y^2} + \mathbf{D}\frac{\partial^2 \mathbf{f}}{\partial z^2}, \tag{A2}$$

$$(1-A_x)\mathbf{f}^{**} = (1+A_x)(1+A_y)(1+A_z)\mathbf{f}^{\tau},$$
$$(1-A_y)\mathbf{f}^{*} = \mathbf{f}^{**},$$
$$(1-A_z)\mathbf{f}^{\tau+1} = \mathbf{f}^{*}, \tag{A3}$$

where $A_x\mathbf{f} = \frac{\mathbf{D}\Delta t}{2}\partial_x^2\mathbf{f} = \frac{\mathbf{D}\Delta t}{2}\frac{\mathbf{f}_{x-1}-2\mathbf{f}_x+\mathbf{f}_{x+1}}{\Delta x^2}$, Δx is the mesh size in the x direction, and Δt is the time-step size. The same is used for A_y, ∂_y^2, and A_z, ∂_z^2; $\mathbf{f}^{\tau}$ and $\mathbf{f}^{\tau+1}$ are current and next steps respectively.

Then, we solve

$$\frac{\partial \mathbf{f}}{\partial t} = \mathbf{S}(\mathbf{f},t)$$

by the Runge-Kutta fourth-order method and add the result ($\mathbf{f}_{RK4}$) to the first equation in Eq. (A3). That addition step is an element of the method for splitting into physical processes.

Finally, we solve resulting equations by the three-diagonal matrix algorithm, also known as the Thomas algorithm, with the given initial and boundary conditions:

$$(1-A_x)\mathbf{f}^{**} = (1+A_x)(1+A_y)(1+A_z)\mathbf{f}^{\tau} + \mathbf{f}^{\tau}_{RK4},$$
$$(1-A_y)\mathbf{f}^{*} = \mathbf{f}^{**},$$
$$(1-A_z)\mathbf{f}^{\tau+1} = \mathbf{f}^{*}. \tag{A4}$$

APPENDIX B

In order to estimate the dependence of a reaction, taking place at a traveling front, on its speed and thickness, we examine the following piecewise-linear equation:

$$\frac{\partial u}{\partial t} = f(u,x) + D\frac{\partial^2 u}{\partial x^2}, \tag{B1}$$

where

$$f(u,x) = \begin{cases} k(u_0 - u) & \text{for } x \in \left[-\frac{L}{2} - vt, \frac{L}{2} - vt\right], \\ -ku & \text{for } x < -\frac{L}{2} - vt \quad \text{and} \quad x > \frac{L}{2} - vt. \end{cases}$$

We seek the automodel solution $u = u(\xi)$ of this equation, where $\xi = x - vt$. Thus, we obtain the following equation:

$$\begin{aligned} &Du''_{\xi\xi} + vu'_{\xi} + k(u_0 - u) = 0, \quad \xi \in \left[-\frac{L}{2}, \frac{L}{2}\right], \\ &Du'_{\xi\xi} + vu'_{\xi} - ku = 0, \quad \xi < -\frac{L}{2} \quad \text{and} \quad \xi > \frac{L}{2}. \end{aligned} \tag{B2}$$

Eigenvalues of this equation are roots of the equation

$$D\lambda^2 + v\lambda - k = 0$$

and are the following:

$$\lambda_1 = \frac{-v + \sqrt{4kD + v^2}}{2D}, \quad \lambda_2 = \frac{-v - \sqrt{4kD + v^2}}{2D}. \tag{B3}$$

A general solution of Eq. (B2) is given by

$$\begin{aligned} u &= ae^{\lambda_1 \xi} && \text{for } \xi < -\frac{L}{2}, \\ u &= be^{\lambda_1 \xi} + ce^{\lambda_2 \xi} && \text{for } \xi \in \left[-\frac{L}{2}, \frac{L}{2}\right], \\ u &= de^{\lambda_2 \xi} && \text{for } \xi > \frac{L}{2}. \end{aligned}$$

Applying the condition of continuity for the function u and its derivative, we determine constants a, b, c, and d.

Thus, the solution of Eq. (B2) in the interval $[-\frac{L}{2}, \frac{L}{2}]$ is the following:

$$u = u_0\left[1 - \frac{\lambda_1}{\lambda_1 - \lambda_2} e^{\lambda_2(\xi + \frac{L}{2})} + \frac{\lambda_2}{\lambda_1 - \lambda_2} e^{\lambda_1(\xi - \frac{L}{2})}\right]. \tag{B4}$$

The maximal value of u in this interval is reached in the point $\xi = \frac{(\lambda_1 + \lambda_2)L}{2(\lambda_1 - \lambda_2)}$ and is equal to

$$\begin{aligned} u &= u_0\left[1 - \exp\frac{\lambda_1 \lambda_2 L}{\lambda_1 - \lambda_2}\right] \\ &= u_0\left[1 - \exp\left(-\frac{kL}{\sqrt{4kD + v^2}}\right)\right]. \end{aligned} \tag{B5}$$

From Eq. (B5), it follows that thickness L of the traveling layer significantly influences the value of u if it is smaller than the value $L_0 \approx \sqrt{4kD + v^2}/k$. While the speed of the front is small ($v \lesssim 2\sqrt{kD}$), its critical thickness L_0 does not depend on the former and in fact is determined by the diffusion length $2\sqrt{D/k}$ of Eq. (B1). For larger values of v, it grows, as is observed in Figs. 2 and 4.

[1] D. Walgraef, *Spatio-Temporal Pattern Formation with Examples from Physics, Chemistry, and Materials Science* (Springer Science & Business Media, Berlin, 2012).

[2] V. Mendez, S. Fedotov, and W. Horsthemke, *Reaction-Transport Systems: Mesoscopic Foundations, Fronts, and Spatial Instabilities* (Springer Science & Business Media, Berlin, 2010).

[3] A. Zaikin and A. Zhabotinsky, Concentration wave propagation in two-dimensional liquid-phase self-oscillating system, Nature (London) **225**, 535 (1970).

[4] M. C. Cross and P. C. Hohenberg, Pattern formation outside of equilibrium, Rev. Mod. Phys. **65**, 851 (1993).

[5] I. R. Epstein and J. A. Pojman, *An Introduction to Nonlinear Chemical Dynamics: Oscillations, Waves, Patterns, and Chaos* (Oxford University Press, Oxford, UK, 1998).

[6] E. Karsenti, Self-organization in cell biology: A brief history, Nat. Rev. Mol. Cell Biol. **9**, 255 (2008).

[7] S. Camazine, J.-L. Deneubourg, N. R. Franks, J. Sneyd, E. Bonabeau, and G. Theraula, *Self-Organization in Biological Systems* (Princeton University Press, Princeton, NJ, 2003).

[8] A. Bayliss and B. J. Matkowsky, Bifurcation, pattern formation, and chaos in combustion, in *Dynamical Issues in Combustion Theory*, edited by P. C. Fife, A. Liñán, and F. Williams (Springer, New York, 1991), pp. 1–35.

[9] G. I. Sivashinsky, Instabilities, pattern formation, and turbulence in flames, Annu. Rev. Fluid Mech. **15**, 179 (1983).

[10] A. I. Volpert and V. A. Volpert, Traveling-wave solutions of parabolic systems with discontinuous nonlinear terms, Nonlin. Anal. **49**, 113 (2002).

[11] Y. Ju and K. Maruta, Microscale combustion: Technology development and fundamental research, Prog. Energy Combust. Sci. **37**, 669 (2011).

[12] R. Liesegang, Ueber einige eigenschaften von gallerten, Naturwissensch. Wochenschr. **11**, 353 (1896) [in German].

[13] A. Merzhanov and I. Borovinskaya, Self-spreading high-temperature synthesis of refractory inorganic compounds, Dokl. Akad. Nauk SSSR, Seriya Khimiya **204**, 366 (1972) [in Russian].

[14] G. I. Sivashinsky, Diffusional–thermal theory of cellular flames, Combust. Sci. Technol. **15**, 137 (1977).

[15] B. J. Matkowsky and G. I. Sivashinsky, Propagation of a pulsating reaction front in solid fuel combustion, SIAM J. Appl. Math. **35**, 465 (1978).

[16] B. J. Matkowsky and D. O. Olagunju, Propagation of a pulsating flame front in a gaseous combustible mixture, SIAM J. Appl. Math. **39**, 290 (1980).

[17] L. Landau, On the theory of slow combustion, JETP **14**, 240 (1944) [in Russian].

[18] J. Buckmaster, Stability of the porous plug burner flame, SIAM J. Appl. Math. **43**, 1335 (1983).

[19] V. Gubernov, V. Bykov, and U. Maas, Hydrogen/air burner-stabilized flames at elevated pressures, Combust. Flame **185**, 44 (2017).

[20] S. Kumar, K. Maruta, S. Minaev, and R. Fursenko, Appearance of target pattern and spiral flames in radial microchannels with CH_4-air mixtures, Phys. Fluids **20**, 024101 (2008).

[21] Y. B. Zeldovich, G. I. Barenblatt, V. B. Librovich, and G. M. Makhviladze, *The Mathematical Theory of Combustion and Explosions* (Consultants Bureau, New York, 1985).

[22] M. El-Hamdi, M. Gorman, J. W. Mapp, and J. I. Blackshear JR, Stability boundaries of periodic models of propagation in burner-stabilized methane-air flames, Combust. Sci. Technol. **55**, 33 (1987).

[23] M. Gorman, C. F. Hamill, M. El-Hamdi, and K. A. Robbins, Rotating and modulated rotating states of cellular flames, Combust. Sci. Technol. **98**, 25 (1994).

[24] M. Gorman, M. El-Hamdi, and K. A. Robbins, Chaotic dynamics near the extinction limit of a premixed flame on a porous plug burner, Combust. Sci. Technol. **98**, 47 (1994).

[25] H. Pearlman, Excitability in high-Lewis-number premixed gas combustion, Combust. Flame **109**, 382 (1997).

[26] V. N. Kurdyumov and M. Sánchez-Sanz, Influence of radiation losses on the stability of premixed flames on a porous-plug burner, Proc. Combust. Inst. **34**, 989 (2013).

[27] S. B. Margolis, Bifurcation phenomena in burner-stabilized premixed flames, Combust. Sci. Technol. **22**, 143 (1980).

[28] S. K. Scott, J. Wang, and K. Showalter, Modelling studies of spiral waves and target patterns in premixed flames, J. Chem. Soc., Faraday Trans. **93**, 1733 (1997).

[29] H. G. Pearlman and P. D. Ronney, Near-limit behavior of high-Lewis number premixed flames in tubes at normal and low gravity, Phys. Fluids **6**, 4009 (1994).

[30] H. G. Pearlman and P. D. Ronney, Self-organized spiral and circular waves in premixed gas flames, J. Chem. Phys. **101**, 2632 (1994).

[31] I. M. Gololobov, E. A. Granovskii, and Y. A. Gostintsev, Two combustion modes at the limit of luminous flame propagation, Combust., Explosion Shock Waves **17**, 22 (1981).

[32] G. Jomaas, J. Bechtold, and C. Law, Spiral waves in expanding hydrogen–air flames: Experiment and theory, Proc. Combust. Inst. **31**, 1039 (2007).

[33] G. Jomaas and C. K. Law, Observation and regime classification of pulsation patterns in expanding spherical flames, Phys. Fluids **22**, 124102 (2010).

[34] G. Wang, Y. Li, W. Yuan, Y. Wang, Z. Zhou, Y. Liu, and J. Cai, Investigation on laminar flame propagation of n-butanol/air and n-butanol/o2/he mixtures at pressures up to 20 atm, Combust. Flame **191**, 368 (2018).

[35] V. K. Vanag and I. R. Epstein, Segmented spiral waves in a reaction-diffusion system, Proc. Natl. Acad. Sci. USA **100**, 14635 (2003).

[36] M. Y. Borina and A. Polezhaev, On the mechanisms for formation of segmented waves in active media, Comput. Res. Model. **5**, 533 (2013).

[37] M. Kuznetsov and A. Polezhaev, The mechanism of formation of oscillons—localized oscillatory structures, Comput. Res. Model. **7**, 1177 (2015).

[38] R. A. Fisher, The wave of advance of advantageous genes, Ann. Eugenics **7**, 355 (1937).

[39] A. Kolmogorov, I. Petrovskii, and N. Piskunov, A study of the equation of diffusion with increase in the quantity of matter, and its application to a biological problem, Moscow Univ. Bull. Math. **1**, 1 (1937).

[40] R. FitzHugh, Mathematical models of threshold phenomena in the nerve membrane, Bull. Math. Biophys. **17**, 257 (1955).

[41] K. Alfaro-Bittner, C. Castillo-Pinto, M. G. Clerc, G. González-Cortés, R. G. Rojas, and M. Wilson, Front propagation into an unstable state in a forced medium: Experiments and theory, Phys. Rev. E **98**, 050201(R) (2018).

[42] E. O. Yakupov and A. A. Polezhaev, Study of the mechanism of the autowave structure formation at the reaction front, Bull. Lebedev Phys. Inst. **45**, 165 (2018).

[43] Y. Ge, F. Zhao, and J. Wei, A high order compact ADI method for solving 3D unsteady convection diffusion problems, Appl. Comput. Math. **7**, 1 (2018).